

Observational Quantification of the Energy Dissipated by Alfvén Waves in a Polar Coronal Hole: Evidence that Waves Drive the Fast Solar Wind.

M. Hahn¹ and D. W. Savin¹

February 22, 2013

Received _____; accepted _____

¹Columbia Astrophysics Laboratory, Columbia University, MC 5247, 550 West 120th Street, New York, NY 10027 USA

ABSTRACT

We present a measurement of the energy carried and dissipated by Alfvén waves in a polar coronal hole. Alfvén waves have been proposed as the energy source that heats the corona and drives the solar wind. Previous work has shown that line widths decrease with height in coronal holes, which is a signature of wave damping, but have been unable to quantify the energy lost by the waves. This is because line widths depend on both the non-thermal velocity v_{nt} and the ion temperature T_{i} . We have implemented a means to separate the T_{i} and v_{nt} contributions using the observation that, at low heights, the waves are undamped and the ion temperatures do not change with height. This enables us to determine the amount of energy carried by the waves at low heights, which is proportional to v_{nt} . We find the initial energy flux density present was $6.7 \pm 0.7 \times 10^5 \text{ erg cm}^{-2} \text{ s}^{-1}$, which is sufficient to heat the coronal hole and accelerate the solar wind during the 2007 - 2009 solar minimum. Additionally, we find that about 85% of this energy is dissipated below $1.5 R_{\odot}$, sufficiently low that thermal conduction can transport the energy throughout the coronal hole, heating it and driving the fast solar wind. The remaining energy is roughly consistent with what models show is needed to provide the extended heating above the sonic point for the fast solar wind. We have also studied T_{i} , which we found to be in the range of 1 - 2 MK, depending on the ion species.

1. Introduction

One of the major models to describe the heating of the solar corona and the acceleration of the solar wind relies on waves to carry the energy. Such wave-driven models have been

supported by observations that waves, particularly Alfvénic waves (Van Doorsselaere et al. 2008; Goossens et al. 2009), are observed throughout the solar atmosphere from the chromosphere (Jess et al. 2009; De Pontieu et al. 2007; McIntosh et al. 2011), to the corona (Tomczyk et al. 2007), and into the solar wind (Belcher & Davis 1971).

However, one difficulty for simple wave-driven models has been that Alfvén waves are predicted to dissipate via viscosity, thermal conductivity, and resistivity relatively far from the Sun, at about 2 - 5 R_{\odot} (e.g., Parker 1991; Cranmer 2002). In order for waves to heat the corona they must be damped at much lower heights where heat conduction is more efficient. For this reason theories have been developed for how the waves may dissipate more quickly. These theories rely on the inhomogeneity of the corona and show, for example, that the waves can be more strongly damped through phase mixing (Heyvaerts & Priest 1983), turbulent cascade (Matthaeus et al. 1999), or resonant absorption (Goossens et al. 2011).

Only recently has incontrovertible observational evidence for dissipation of Alfvén waves at low heights been found. Hahn et al. (2012) and Bemporad & Abbo (2012) studied coronal hole observations and demonstrated that Alfvén waves are damped at relatively low heights in the corona. In these studies the Alfvén waves were observed spectroscopically through the non-thermal broadening of optically thin spectral lines. The magnitude of the non-thermal broadening is predicted to be proportional to the wave amplitude (Banerjee et al. 1998; Doyle et al. 1998; Moran 2001; Banerjee et al. 2009). For energy to be conserved the wave amplitude must increase with height above the Sun as the density decreases. Hahn et al. (2012) and Bemporad & Abbo (2012) found that the line widths decrease above about 1.2 R_{\odot} . They ruled out systematic errors as the cause of the decrease. This confirmed some earlier indications that the line widths decrease at larger heights (Banerjee et al. 1998; Doyle et al. 1999; Moran 2003; O’Shea et al. 2005; Dolla & Solomon 2008).

In order to determine if waves are indeed responsible for heating the corona and driving the solar wind one must quantify both the energy initially present in the waves as well as that dissipated by the waves. This has been difficult to determine because the measurement of a line width includes contributions both from thermal broadening, which is proportional to the ion temperature T_i , and from non-thermal broadening, which is proportional to the non-thermal velocity v_{nt} . A conventional method to estimate v_{nt} is to assume some value for T_i . For example, Bemporad & Abbo (2012) assumed the ion temperature was equal to the ionization equilibrium formation temperature of the ion emitting the line. However, this is not necessarily correct since some studies have shown that T_i may be much greater than the formation temperature (e.g., Tu et al. 1998; Landi & Cranmer 2009; Hahn et al. 2010). Because T_i is expected to be larger than T_e , Hahn et al. (2012) assumed that $T_i = T_e$ and thereby estimated an upper bound for v_{nt} .

Here we present in Section 3 a method to separately determine v_{nt} and T_i . The v_{nt} data are presented in Section 4. The non-thermal velocity is proportional to the wave amplitudes and from it we determine the initial wave energy, the change in the wave energy flux density, and the length and time scales over which the waves are damped. These data indicate that waves are sufficient to heat the coronal hole and drive the fast solar wind. They also provide quantitative constraints for theoretical models of wave damping. In Section 5 we present our measurements of ion temperatures and compare them to some earlier measurements that found only lower and upper bounds for the temperature. These temperature data can be used to test various models for resonant ion heating in the corona.

2. Observation

Our data come from four observations made with the Extreme ultraviolet Imaging Spectrometer (EIS; Culhane et al. 2007) on *Hinode* (Kosugi et al. 2007). The observations

were made on 2009 April 23 at 12:42, 13:16, 13:50, and 15:17. Each observation was 30 minutes in duration. For these data the 2'' slit was pointed at a polar coronal hole at positions relative to the central meridian of $X = -14.5'', 15.5'', 45.4'',$ and $105.6'',$ respectively. The height range covered by the slit extended from about $0.95 R_{\odot}$ to about $1.45 R_{\odot}$. These data are the same as used by Hahn et al. (2012), but excluding their observation centered at $X = -44.5''$. We omitted that particular observation as it had a larger density scale height at low heights compared to the other pointings, possibly due to intervening quiet Sun material. Our results for wave damping, though, are consistent with the previous results that included the additional observation.

The four pointings were averaged together in order to improve the statistical accuracy. This was done by first using the standard EIS processing routines to clean the data of spikes, warm pixels, and dark current, and calibrate the data. Drifts in the wavelength scale were then corrected using the method described by Kamio et al. (2010). After aligning the data to the same wavelength scale, pixels at the same radius from each of the four observations were averaged to create the dataset analyzed. Finally, these data were further binned in the vertical direction. For the the analysis described below, where we perform a fit to the data at low heights, we have used a binning of 8 pixels per bin ($\sim 0.01 R_{\odot}$). To extend these results to larger heights, where the intensities are correspondingly much smaller, we have used a 32 pixel binning ($\sim 0.03 R_{\odot}$).

3. Analysis Method

3.1. Line Widths

We fit Gaussian functions to the spectrum in order to derive the line widths. In particular, each line was fit with a double Gaussian in order to account for instrument

scattered light. The lines used for various aspects of the analysis are given in Table 1. The fitting procedures are described in detail in Hahn et al. (2012), so here we only briefly review the method.

Stray light is the unshifted spectrum of solar disk emission that is scattered by the instrumental optics onto the off-disk data. Because line widths tend to be narrower on the disk, scattered light can be a significant source of systematic error at large heights when the fraction of real emission is small. To correct for the scattered light we first measured line profiles from the portions of our observation that looked at the solar disk. Then we constructed a predicted scattered light line profile for each line. For these parameters we used the measured line width and centroid position and 2% of the on-disk intensity. This last value is based on estimates for the magnitude of the scattered light EIS (Ugarte 2010; Hahn et al. 2012). Then, for each position in the off-disk data, a fit was performed using a Gaussian with free parameters added to this artificial scattered light profile. This is equivalent to subtracting the scattered light profile from the spectrum.

The measured full width at half maximum $\Delta\lambda_{\text{FWHM}}$ of an optically thin spectral line depends on instrumental broadening $\Delta\lambda_{\text{inst}}$, the ion temperature T_i , and the non-thermal velocity v_{nt} as (Phillips et al. 2008)

$$\Delta\lambda_{\text{FWHM}} = \left[\Delta\lambda_{\text{inst}}^2 + 4 \ln(2) \left(\frac{\lambda}{c} \right)^2 \left(\frac{2k_B T_i}{M} + v_{\text{nt}}^2 \right) \right]^{1/2}. \quad (1)$$

Here λ is the wavelength of the line, c is the speed of light, k_B is the Boltzmann constant, and M is the mass of the ion. We have subtracted the instrumental width using the tabulated $\Delta\lambda_{\text{inst}}$ values as a function of position along the slit (Young 2011). The observed width can then be expressed as an effective velocity,

$$v_{\text{eff}} = \sqrt{v_{\text{th}}^2 + v_{\text{nt}}^2}, \quad (2)$$

where $v_{\text{th}} = \sqrt{2k_B T_i / M}$. This v_{eff} depends on both T_i and v_{nt} .

3.2. Separating Thermal and Non-thermal Broadening

Dolla & Solomon (2008) pointed out that the thermal and non-thermal contributions can be inferred if two assumptions are made. One can then calculate $v_{\text{nt}}(R_0)$ at a radius R_0 using data from another height R_1 . The first assumption is that v_{th} is constant with height for each ion emitting the line being studied. This implies that

$$v_{\text{eff}}^2(R_1) - v_{\text{eff}}^2(R_0) = v_{\text{nt}}^2(R_1) - v_{\text{nt}}^2(R_0). \quad (3)$$

The other assumption is that the waves are undamped. Moran (2001) has shown that this conservation of energy then implies that $v_{\text{nt}} \propto n_e^{-1/4}$. Since the waves are assumed to be undamped we have

$$\frac{v_{\text{nt}}(R_1)}{v_{\text{nt}}(R_0)} = \left[\frac{n_e(R_1)}{n_e(R_0)} \right]^{-1/4}. \quad (4)$$

Putting it all together, one finds

$$v_{\text{nt}}(R_0) = \left\{ \frac{v_{\text{eff}}^2(R_1) - v_{\text{eff}}^2(R_0)}{\left[\frac{n_e(R_1)}{n_e(R_0)} \right]^{-1/2} - 1} \right\}^{1/2}. \quad (5)$$

Dolla & Solomon (2008) used this method to determine $v_{\text{nt}}(R_0)$ by taking an average over the results for a fixed R_0 while varying R_1 . However, they did not observe damping and they inferred a quite small v_{nt} , possibly for the reasons we discuss below in Section 4.

The method we use relies on the same assumptions as the Dolla & Solomon (2008) method, but the application is somewhat different. Here, we use a least squares fit. The reason for doing this is that uncertainties in the data can cause large variations in the $v_{\text{nt}}(R_0)$ determined using equation (5). A least squares fit takes these uncertainties into account implicitly and is more robust to noise. Combining equations (2), (3), and (4), the function used in the fit is

$$v_{\text{eff}}(R) = \sqrt{v_{\text{th}}^2 + v_{\text{nt}}^2(R_0) \left[\frac{n_e(R)}{n_e(R_0)} \right]^{-1/2}}. \quad (6)$$

Here, v_{th} and $v_{nt}(R_0)$ are the only free parameters to be determined. As we discuss later, we assume that v_{th} for a given ion is the same for every height, though it can be different for each ion. Solving equations (5) or (6) requires the ratio $n_e(R)/n_e(R_0)$. We describe below how this is determined.

The assumption of constant ion temperature is reasonable for low heights. Ions in coronal holes are known to be heated, although the precise mechanism has not been determined. Some possibilities include ion cyclotron resonance heating by high frequency waves (Cranmer 2002) and stochastic heating by turbulent fluctuations that disturb the ion orbits (Chandran 2010). In either case the heating rate is predicted to depend on the charge to mass ratio, with minor ions heated more strongly than protons. For this reason, at low heights Coulomb collisions with the protons are expected to cool the ions and maintain them at a relatively steady temperature (Landi & Cranmer 2009). Measurements estimating upper and lower bounds for T_i at heights of $R \lesssim 1.15 R_\odot$ have shown that T_i is consistent with being constant over this height range, albeit with large uncertainties (Landi & Cranmer 2009; Hahn et al. 2010). Note that each ion may have a different T_i or v_{th} , both of which we assume do not change with height.

It is also reasonable to assume that waves are undamped at low heights, and consequently $v_{nt} \propto n_e^{-1/4}$. This theoretical relation is valid for outward propagating waves when the solar wind velocity is much smaller than the Alfvén speed (Cranmer & van Ballegoijen 2005), a condition expected to be met at low heights. Numerous studies have observed the predicted trend for $R \lesssim 1.15 R_\odot$ (Doyle et al. 1998; Banerjee et al. 1998, 2009; Hahn et al. 2012; Bemporad & Abbo 2012). In estimating v_{nt} , these studies have assumed T_i to be either the ion formation temperature or the electron temperature, but have found the same $n_e^{-1/4}$ trend. Thus, this trend is not very sensitive to uncertainties in the magnitude of T_i .

Based on the above, in the range $1.02 - 1.12 R_\odot$ the ion temperatures should be

reasonably constant with height; although, T_i may still differ depending on the ion species. Also, the upper height of $1.12 R_\odot$ is below the point where the waves appear to be damped. Thus, it is reasonable to perform the fits to equation (6) over these heights.

Our analysis also requires an independent measurement of n_e . This was obtained from the intensity ratio of the Fe IX 188.50 Å and 189.94 Å lines using atomic data from CHIANTI (Dere et al. 1997; Landi et al. 2012). Figure 1 shows the inferred densities, which are typical of densities found in other coronal hole observations (Wilhelm et al. 2011). At these low heights the solar wind velocity is small and the corona is close to hydrostatic equilibrium. We therefore fit the density over the range $1.02 - 1.12 R_\odot$ using (e.g., Guhathakurta et al. 1992; Doyle et al. 1999)

$$n_e(R) = n_e(R_0) \exp \left[\frac{-(R - R_0)}{H R_0 R} \right], \quad (7)$$

where H is the density scale height, which was found to be $H = 0.0657 \pm 0.0052 R_\odot$. (Here and throughout we give the 1σ uncertainties.) The fit is illustrated in figure 1. Using this expression for the density, the ratio $n_e(R)/n_e(R_0)$ in equation 6 can be rewritten so that

$$v_{\text{eff}}(R) = \sqrt{v_{\text{th}}^2 + v_{\text{nt}}^2(R_0) \left[\exp \frac{-(R - R_0)}{R R_0 H} \right]^{-1/2}}. \quad (8)$$

This function is useful for our analysis as some of the statistical fluctuations in the magnitude of n_e are smoothed out, while retaining the essential description of the density variation with height.

3.3. Uncertainties

Uncertainties in the line widths v_{eff} and H were propagated into the fitted parameters v_{th} and v_{nt} using a Monte Carlo analysis. The observed data for each fit are the single inferred value of H and a set of values for v_{eff} as a function of height for a given ion.

Normally distributed random variations were added to these input data. The magnitude of these variations was set so that the standard deviation of the random numbers added was equal to the 1σ uncertainty for each data point used in the fit of equation (8) over the height range 1.02 - 1.12 R_\odot (e.g., Figure 2). The fits were then performed for 1000 different variations, with each iteration producing different v_{th} and v_{nt} . Next we took the mean of each parameter and estimated the 1σ uncertainty to be the standard deviation.

We found that for some of the iterations, the value of v_{th} for a given ion would imply $T_i < T_e$. Although this is clearly a possible fit to the data, the result does not seem physically reasonable. At very low heights, below the range of our fit, the density is high enough that electrons, protons, and ions should be in equilibrium so that $T_i = T_e$. At large heights the ions are observed to be heated and $T_i > T_e$ and collisions can be neglected. In the range where we perform the fits, the situation lies in-between these two extremes, that is the ions are expected to be heated in some way, but also to be cooled by collisions with protons having $T_p \geq T_e$ (Esser et al. 1999; Landi & Cranmer 2009; Hahn & Savin 2013). Thus, throughout the observed height range we expect $T_i \geq T_e$. We have applied this constraint to our analysis by rejecting fits that imply $T_i < 8 \times 10^5$ K, which is consistent with a previous analysis of this observation (Hahn et al. 2012) and is a typical T_e for a coronal hole (Wilhelm et al. 2011).

4. Wave Amplitude and Energy

Fits to equation (8) were performed over the range 1.02 - 1.12 R_\odot . The fits used a total of eleven lines from five ions (see column three of Table 1). Figure 2 shows an example of the fit for Fe XI. If all the lines originate from the same volume, then it is expected that they will all have the same v_{nt} , though not necessarily the same v_{th} . As expected, the inferred v_{nt} from the five different ions were in reasonable agreement with one another

(Table 2). Thus, took the unweighted mean of the results from the different ions to find that $v_{\text{nt}} = 33.0 \pm 2.4 \text{ km s}^{-1}$ at $1.05 R_{\odot}$.

In the study of Dolla & Solomon (2008) they found $v_{\text{nt}} = 15 \pm 2 \text{ km s}^{-1}$, which is significantly smaller than we find here. There are several possible explanations for this apparent discrepancy. Dolla & Solomon (2008) focussed on an observation made in May 2002. This time period was near solar maximum, whereas our data were obtained near solar minimum and so the difference may reflect some solar cycle variation. Additionally, they described the polar coronal hole as “not well developed” and so their data likely contains other structures along the line of sight. For their analysis they studied a line from Mg x, which is a lithium-like ion with a peak formation $T_e \approx 1.3 \times 10^6 \text{ K}$, but also has a tail of high ion abundance towards much greater temperatures (Bryans et al. 2009). Thus, if v_{nt} is smaller in hotter structures than it is in a coronal hole, then their value would be systematically underestimated.

Figure 3 shows v_{nt} as a function of R for Si VII 275.37 Å, Fe IX 197.86 Å, Fe X 184.54 Å, and Fe XI 188.22 Å. These lines, listed in the fourth column of Table 1, were chosen because they could be observed to relatively large heights. In each case the corresponding v_{th} from Table 2 has been subtracted from v_{eff} using the values for each ion determined from the fits (see Table 2). The solid line in the figure shows the mean $v_{\text{nt}}(R)$ in $0.03 R_{\odot}$ bins for these lines and the dashed line shows the predicted $n_e^{-1/4}$ trend for undamped waves. The data show that v_{nt} is consistent with undamped waves below about $1.15 R_{\odot}$. However, at larger heights v_{nt} deviates from this profile, which implies wave damping.

The energy density flux carried by the waves can be estimated using (Doyle et al. 1998; Banerjee et al. 1998; Moran 2001)

$$F = 2\rho v_{\text{nt}}^2 V_A,$$

where ρ is the mass density and

$$V_A = B/\sqrt{4\pi\rho}$$

is the Alfvén speed with B being the magnetic field strength. To estimate the varying magnetic field strength for the superradially expanding polar coronal hole we used the empirical model from equation (6) of Cranmer et al. (1999b). In terms of the area expansion $A(R)/A(R_\odot)$ this gives

$$B(R) = B(R_\odot)A(R_\odot)/A(R).$$

Wang (2010) gives $B(R_\odot) = 7.3$ G for this solar minimum. Other measurements show that the polar magnetic field can vary by a few Gauss between solar cycles (Wang et al. 2009), so we estimate the uncertainty within a single solar minimum to be about 1 G. At low heights ρ can be found from the measured n_e . For larger heights it was necessary to extrapolate the density measurements. We did this using the profile from Cranmer & van Ballegooijen (2005) which was based on white light measurements out to several R_\odot . Their $n_e(R)$ function was scaled to match our measurements at $1.12 R_\odot$. The uncertainty of the scaling factor was taken to match that of n_e at $1.12 R_\odot$. Additionally, we found that F remains nearly identical if we simply use the hydrostatic fit for n_e over the entire height range.

Figure 4 shows the energy density flux F as a function of height based on the averaged results for v_{nt} , plotted in Figure 3. These data are also listed in Table 3. The error bars represent the combined uncertainties from v_{nt} , ρ and B . One can see that F is decreasing with height, but some of this decrease is due simply to the expansion of the coronal hole. The dashed line in Figure 4 illustrates the variation of F with height for undamped waves, where the decrease is due only to the superradial expansion of the coronal hole (Cranmer et al. 1999b). Clearly the waves are damped more rapidly with height than predicted by expansion alone.

To more clearly show the effect of damping we show the quantity $FA(R)/A(R_\odot)$ in

Figure 5 (also listed in Table 3). In this plot, measurements for undamped waves would fall on a horizontal line. The data are consistent with undamped waves for $R \lesssim 1.15 R_\odot$. The dashed line in Figure 5 is drawn at the average of the points below $1.12 R_\odot$, which is $F = 6.7 \pm 0.7 \times 10^5 \text{ erg cm}^{-2} \text{ s}^{-1}$. This is the amount of Alfvén wave energy present at the base of the corona. Withbroe & Noyes (1977) estimated that $8 \times 10^5 \text{ erg cm}^{-2} \text{ s}^{-1}$ is typically required to heat a coronal hole and accelerate the fast solar wind. However, during the 2007 - 2009 solar minimum the solar wind was observed to be unusually weak, being about 25% less energetic than in previous minima (McComas et al. 2008; Wang 2010). This implies that for the recent solar minima only about $6 \times 10^5 \text{ erg cm}^{-2} \text{ s}^{-1}$ would be required. Our measurements show not just that the amount of energy carried by the waves is sufficient to account for coronal heating and solar wind acceleration within the coronal hole. In addition they indicate that the waves are indeed damped, losing $\sim 85\%$ of their initial energy $1.5 R_\odot$ (Figure 5). Thus, our findings indicate that the waves do in fact provide most of the required heating.

The length and time scales over which the waves are damped provide benchmarks for theoretical calculations. In order to estimate the length scale over which the waves are damped we fit an exponential to $FA(R)/A(R_\odot)$. This fit is illustrated by the solid line in Figure 5. The initial value of F , the height where damping begins R_d , and the exponential damping length L_d , were free parameters of the fit. The initial F was the same as found above, $F = 6.7 \pm 0.7 \times 10^5 \text{ erg cm}^{-2} \text{ s}^{-1}$. The fit found $R_d = 1.12 \pm 0.04 R_\odot$, which is consistent with the point where v_{nt} deviates from the $n_e^{-1/4}$ trend (e.g., Figure 3). The relatively large error bar is due to the course binning used here. We find that the damping length is about $L_d = 0.18 \pm 0.04 R_\odot$. We can also estimate a timescale for the damping. Since the velocity of the waves is about the Alfvén speed, we can convert R to wave travel time t . Fitting an exponential to the data as a function of t , we find that the damping time is about $68 \pm 15 \text{ s}$.

Solar wind models show that in order to accelerate the fast solar wind to the speeds observed far from the Sun, some input of wave energy is needed above the point where the solar wind becomes supersonic (Cranmer 2002). This suggests that not all of the wave energy should be damped at very low heights. The amount of initial energy that is required to be undamped to large heights is about $1 \times 10^5 \text{ erg cm}^{-2} \text{ s}^{-1}$. Our results show that at least up to about $1.4 R_{\odot}$ sufficient energy remains in the waves to provide the additional acceleration for the solar wind. However, because of the large uncertainties, our data can also be consistent with the wave energy going to zero at large distances. To get a rough estimate we performed a similar fit to the one described in the above paragraph, but using an exponential plus a constant. We find that at large distances $FA(R)/A(R_{\odot}) \rightarrow 0.6 \pm 1.4 \times 10^5 \text{ erg cm}^{-2} \text{ s}^{-1}$. One additional source of uncertainty for this estimate is that we do not know how the ion temperatures are changing with height. As the dissipation of the wave energy is likely to heat the ions, the assumption of constant temperature is probably becomes less reasonable at the larger heights in our observation. Since any resulting thermal broadening would increase with height, our assumption of constant v_{th} would cause us to underestimate the actual damping.

5. Ion Temperatures

The temperature of each ion can be inferred at $1.05 R_{\odot}$ from all the line widths observed at that height (column five of Table 1) by subtracting the non-thermal width $v_{\text{nt}} = 33.0 \pm 2.4 \text{ km s}^{-1}$. The circles in Figure 6 shows T_{i} for each of the ions measured as a function of charge to mass ratio q/M , in units of elementary charge e per atomic mass unit (amu). These data are also given in Table 4.

Previous measurements have found that T_{i} is greater than T_{e} for $q/M \lesssim 0.2$, while for slightly higher q/M ions $T_{\text{i}} \approx T_{\text{e}}$, but may increase again for $q/M \gtrsim 0.3$ (Landi & Cranmer

2009; Hahn et al. 2010). Here we find a similar pattern with respect to q/M . For $q/M < 0.2$ $T_i \approx 2 \times 10^6$ K, while for larger q/M $T_i \approx 1 \times 10^6$ K, which is about the expected value of T_e for a coronal hole. For larger $q/M > 0.3$ there is a suggestion that T_i increases if one looks at the S X and O VI data. The yet higher q/M point from Si X might appear to contradict this trend, but this could be a systematic error since Si X is formed at relatively high temperatures and so a large fraction of the emission may come from structures outside the coronal hole (Hahn et al. 2012). We should also note that our uncertainties are large enough that we cannot rule out that T_i is actually constant over the entire range with respect to q/M .

Different models for ion heating predict different dependences of T_i on q/M . Thus, T_i measurements can be used to test these models. For example, Cranmer et al. (1999a) developed a model in which the ions are heated by ion cyclotron waves. Based on their equations (2) and (15), ignoring collisions, and assuming a typical solar wind plasma wave spectral index of 3/2 (Leamon et al. 1998; Podesta et al. 2007; Chandran 2010) one finds

$$T_i \propto M \left(\frac{q}{M} \right)^{1/2} \left(1 - \frac{q}{M} \right). \quad (9)$$

Another model is that of Chandran (2010) in which Alfvén wave turbulence causes ion orbits to become stochastic and absorb energy from the turbulence. They derive a dependence of T_i on q/M if (a) the ratio of the turbulent velocity fluctuations to the thermal velocity perpendicular to the magnetic field are the same for all the ions, (b) the turbulent fluctuations have spectral index 3/2, and (c) collisions can be ignored, finding that

$$T_i \propto M \left(\frac{M}{q} \right)^{2/3}. \quad (10)$$

However, the neglect of collisions in deriving both of these trends is probably not a very good approximation at these low heights. Nevertheless, we can compare these predictions to our data. The open squares and diamonds in Figure 6 illustrate the predicted trends

from Cranmer et al. (1999a) and Chandran (2010), respectively. In each case the theoretical trends have been multiplied by a scaling factor that was chosen to produce the best average agreement with the observations. Given the large uncertainties in our analysis and the neglect of collisions in the models, both predictions show reasonable agreement with our data.

6. Summary

We have shown that Alfvén waves in a polar coronal hole possess sufficient energy to heat the coronal hole and that this energy is actually dissipated from the waves at sufficiently low heights. To show this we determined separately the thermal and non-thermal components of spectral line broadening in a coronal hole. Our method relies on the observation that waves are undamped at very low heights and on the assumption that the temperature of each ion does not change with height at low heights. From the derived v_{nt} we show that the energy carried by the waves is $6.7 \pm 0.7 \times 10^5 \text{ erg cm}^{-2} \text{ s}^{-1}$, which is sufficient to heat the coronal hole and accelerate the fast solar wind. The waves are damped over a length of about $0.18 \pm 0.04 R_{\odot}$, with a corresponding timescale of about $68 \pm 15 \text{ s}$. Although our measurements are limited to $R < 1.5 R_{\odot}$, they suggest that enough energy remains in the waves to provide the extended heating of the solar wind above the sonic point that models show is required. Additionally, we measured T_i for each ion to be in the range of about 1 - 2 MK. We found a weak trend where low $q/M < 0.2$ ions have the highest temperature, $q/M \approx 0.2 - 0.25$ are lower with $T_i \approx T_e$, and $q/M > 0.25$ have a slightly increasing temperature. Our uncertainties are not sufficiently small to distinguish between the predictions of two ion heating models. Those models are also not realistic for these heights since they neglect Coulomb collisions. Our results, though, do demonstrate that such a comparison is possible in principle, with some additions to the model and higher

quality data.

MH and DWS were supported in part by the NASA Solar Heliospheric Physics program grant NNX09AB25G and the NSF Division of Atmospheric and Geospace Sciences SHINE program grant AGS-1060194.

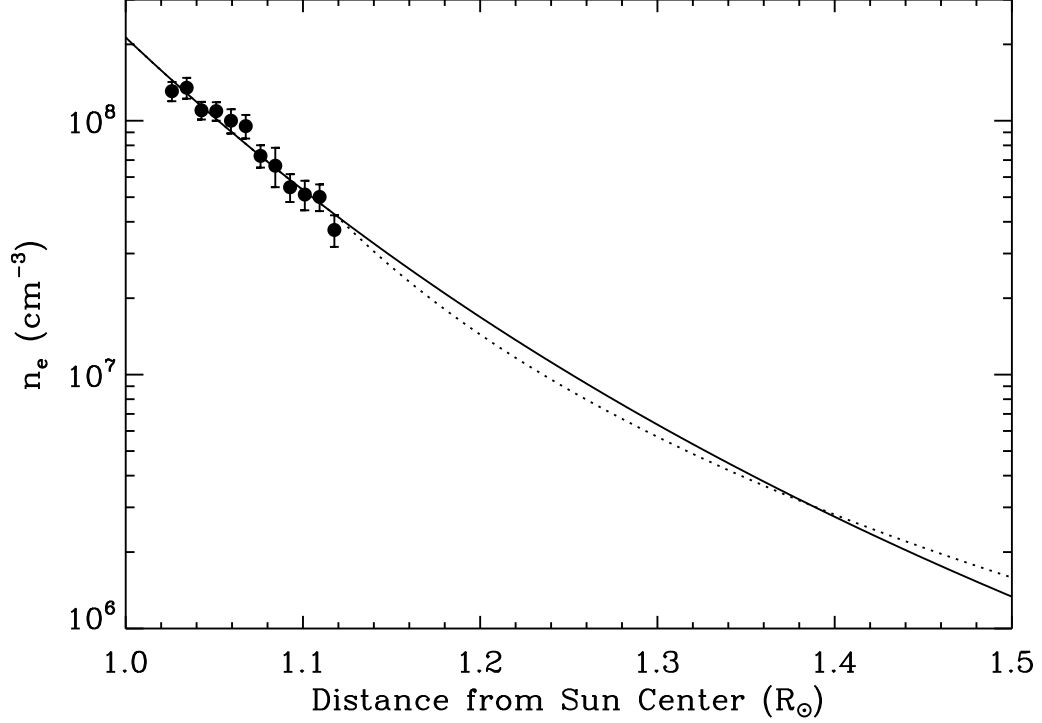


Fig. 1.— The filled circles indicate the electron density n_e derived from an Fe IX intensity ratio. The solid line shows the hydrostatic equilibrium fit to the data using equation (7) in the range $1.02 - 1.12 R_\odot$. The dotted line shows the empirical model from Cranmer & van Ballegoijen (2005), scaled to match the data at $1.12 R_\odot$. For the analysis we used the hydrostatic fit for $R < 1.12 R_\odot$ and extended to larger heights using the empirical model.

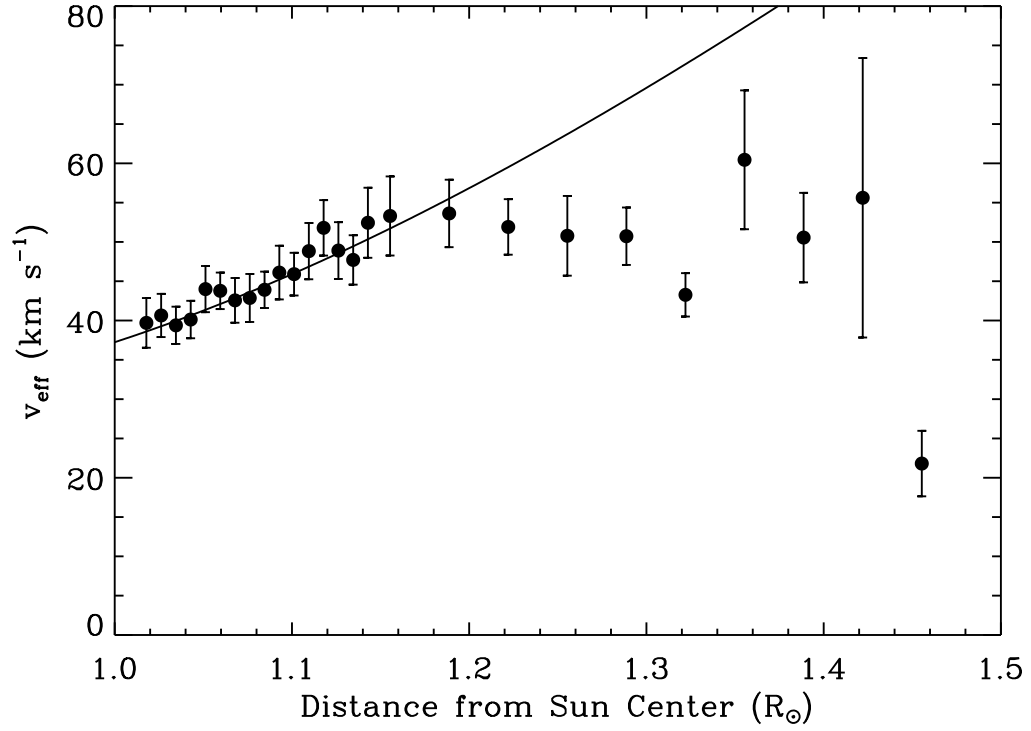


Fig. 2.— The filled circles show the measured effective velocity v_{eff} for Fe XI 188.22 Å. The solid line illustrates the average fit to the data between 1.02 and 1.12 R_{\odot} using equation (8). The fit parameters for this ion were $v_{\text{th}} = 25.8 \pm 5.4 \text{ km s}^{-1}$ and $v_{\text{nt}} = 32.2 \pm 4.2 \text{ km s}^{-1}$.

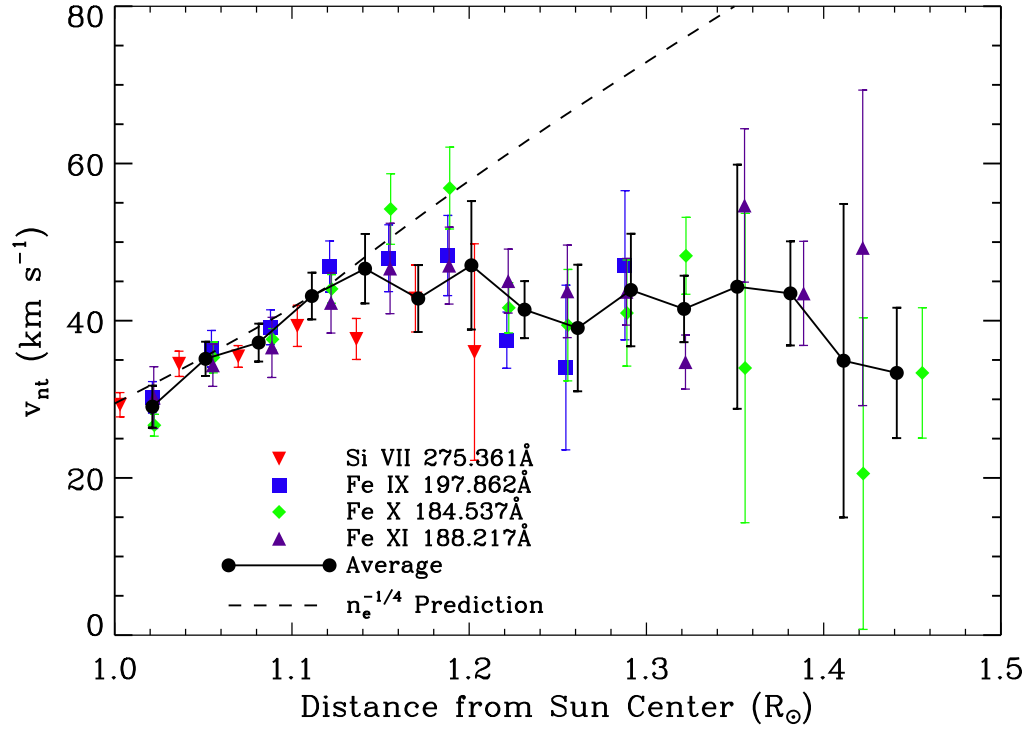


Fig. 3.— Symbols indicate the non-thermal velocity v_{nt} from the strongest observed lines. The filled circles and solid line show the averaged v_{nt} combining the data from the various ions. The dashed line illustrates the predicted electron density $n_e^{-1/4}$ trend for undamped waves.

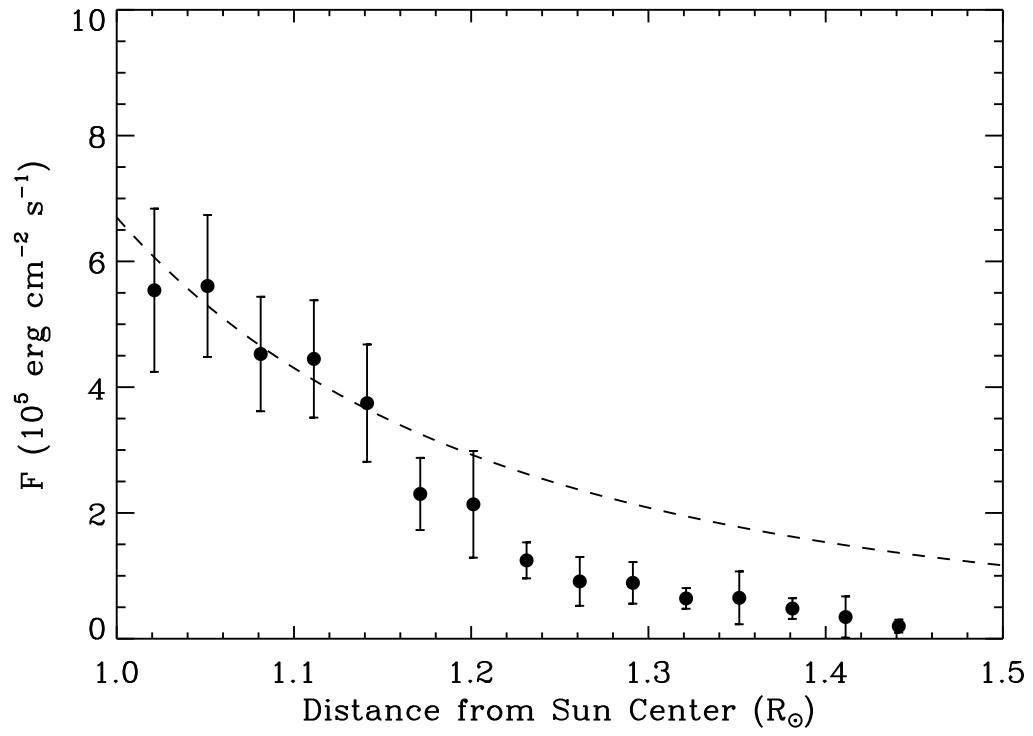


Fig. 4.— Wave energy density flux F as a function of height (filled circles). The dashed line illustrates the predicted trend for undamped waves.

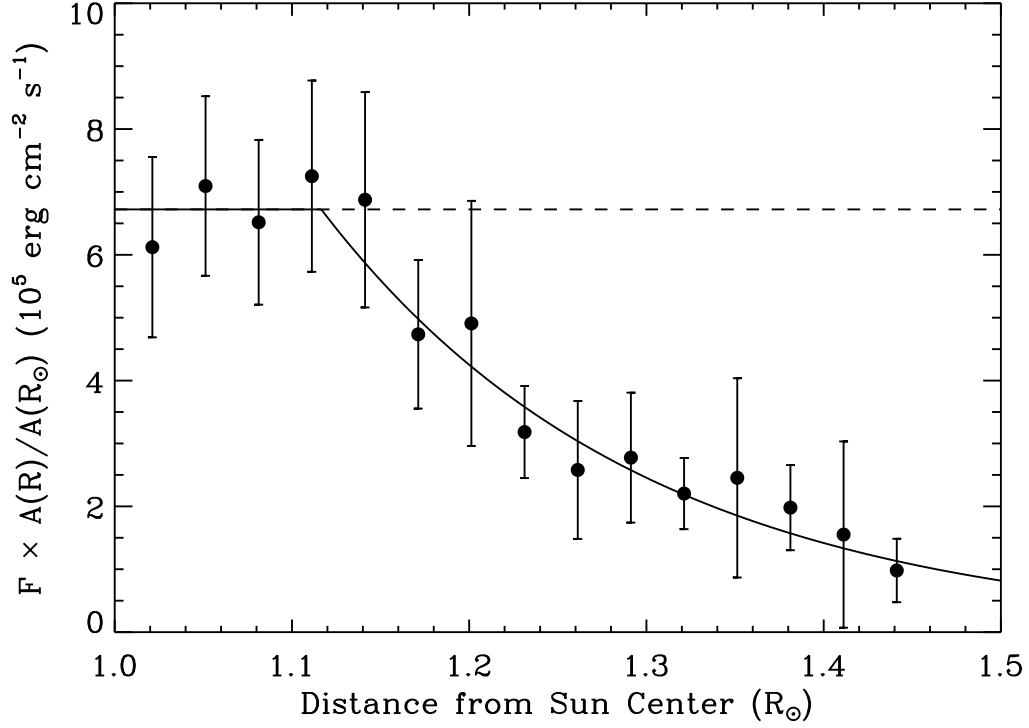


Fig. 5.— Points indicate F multiplied by the expansion factor $A(R)/A(R_\odot)$ in order to more clearly show the decrease due to damping. For undamped waves, the points would fall on a horizontal line. The dashed line indicates the average of the points below $1.12 R_\odot$. This average shows that $F = 6.7 \pm 0.7 \times 10^5 \text{ erg cm}^{-2} \text{ s}^{-1}$ is present in the waves at $1 R_\odot$. The solid line gives an exponential fit, from which a damping length of $0.18 R_\odot$ was derived. The point at which the exponential decay begins was a free parameter of the fit, with the result $R = 1.12 \pm 0.04 R_\odot$.

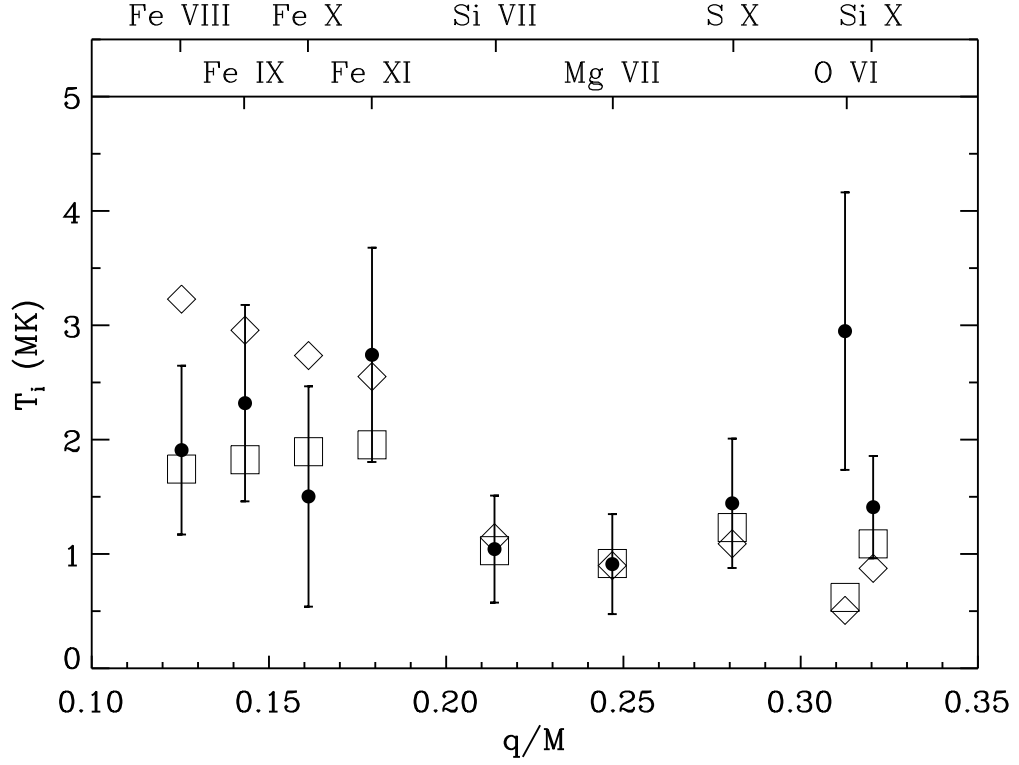


Fig. 6.— Filled circles show the temperature T_i for each ion, derived by subtracting the average $v_{nt} = 33.0 \pm 2.4 \text{ km s}^{-1}$ from v_{eff} , plotted versus charge to mass ratio q/M for different ion species. The open squares and open diamonds show the pattern of T_i versus q/M predicted by the models of Cranmer et al. (1999a) and Chandran (2010), respectively.

Table 1:: Line List.

Ion	λ (Å) ¹	Used for:		
		Eq. (8) Fit	$v_{\text{nt}}(R)$	$T_{\text{i}}(1.05R_{\odot})$
O IV	279.631			*
O IV	279.933			*
Mg VII	276.154			*
Si VII	272.648	*		*
Si VII	275.361	*	*	*
Si VII	275.676	*		*
Si X	258.374			*
Si X	261.057			*
Si X	271.992			*
Si X	277.264			*
Fe VIII	185.213	*		*
Fe VIII	186.599	*		*
Fe VIII	194.661	*		*
Fe IX	188.497	*		*
Fe IX	189.941	*		*
Fe IX	197.862	*	*	*
Fe X	184.537	*	*	*
Fe X	190.037			*
Fe X	193.715			*
Fe X	{ 257.259			*
				*
Fe XI	180.401			*

Ion	λ (Å) ¹	Used for:		
		Eq. (8) Fit	$v_{\text{nt}}(R)$	$T_{\text{i}}(1.05R_{\odot})$
Fe XI	188.217	*	*	*
Fe XI	188.299			... ²

¹Wavelengths from CHIANTI (Dere et al. 1997; Landi et al. 2012).

² $\Delta\lambda$ was constrained to be identical for Fe XI 188.217 Å and 188.299 Å.

⁰Brackets indicate blends from the same ion.

Table 2:: Values for v_{th} and v_{nt} at $1.05 R_{\odot}$ from fitting Equation (8) over 1.02 - 1.12 R_{\odot} .

Ion	v_{th} (km s ⁻¹)	v_{nt} (km s ⁻¹)
Si VII	23.5 ± 1.5	33.6 ± 1.2
Fe VIII	19.9 ± 2.7	29.8 ± 1.8
Fe IX	20.4 ± 3.0	34.9 ± 1.8
Fe X	18.7 ± 2.6	34.5 ± 1.5
Fe XI	25.8 ± 5.4	32.2 ± 4.2

Table 3:: Non-thermal velocity and Energy Flux Density.

$R \ R_{\odot}$	$F \ (10^5 \text{ erg cm}^{-2} \text{ s}^{-1})$	$F \frac{A(R)}{A(R_{\odot})} \ (10^5 \text{ erg cm}^{-2} \text{ s}^{-1})$
1.02	5.5 ± 1.3	6.1 ± 1.4
1.05	5.6 ± 1.1	7.1 ± 1.4
1.08	4.53 ± 0.91	6.5 ± 1.3
1.11	4.45 ± 0.93	7.3 ± 1.5
1.14	3.75 ± 0.93	6.9 ± 1.7
1.17	2.30 ± 0.57	4.7 ± 1.2
1.20	2.14 ± 0.85	4.9 ± 1.9
1.23	1.25 ± 0.29	3.18 ± 0.73
1.26	0.91 ± 0.39	2.6 ± 1.1
1.29	0.89 ± 0.33	2.8 ± 1.0
1.32	0.64 ± 0.16	2.20 ± 0.57
1.35	0.65 ± 0.42	2.5 ± 1.6
1.38	0.48 ± 0.16	1.98 ± 0.68
1.41	0.34 ± 0.33	1.5 ± 1.5
1.44	0.20 ± 0.10	0.98 ± 0.50

Table 4:: Ion Temperatures.

Ion	$q/M \left(\frac{e}{\text{amu}}\right)$	T_i (MK)
O VI	0.31	2.9 ± 1.2
Mg VII	0.25	0.91 ± 0.44
Si VII	0.21	1.04 ± 0.47
Si X	0.32	1.41 ± 0.45
S X	0.28	1.44 ± 0.57
Fe VIII	0.13	1.91 ± 0.74
Fe IX	0.14	2.32 ± 0.86
Fe X	0.16	1.50 ± 0.96
Fe XI	0.18	2.74 ± 0.94

REFERENCES

- Banerjee, D., Pérez-Suárez, D., & Doyle, J. G. 2009, A&A, 501, L15
- Banerjee, D., Teriaca, L., Doyle, J. G., & Wilhelm, K. 1998, A&A, 339, 208
- Belcher, J. W. & Davis, L. 1971, J. Geophys. Res., 76, 3534
- Bemporad, A. & Abbo, L. 2012, ApJ, 751, 110
- Bryans, P., Landi, E., & Savin, D. 2009, ApJ, 691, 1540
- Chandran, B. D. G. 2010, ApJ, 720, 548
- Cranmer, S. R. 2002, Space Sci. Rev., 101, 229
- Cranmer, S. R., Field, G. B., & Kohl, J. L. 1999a, ApJ, 518, 937
- Cranmer, S. R. & van Ballegoijen, A. 2005, ApJS, 156, 265
- Cranmer, S. R. et al. 1999b, ApJ, 511, 481
- Culhane, J. L. et al. 2007, Sol. Phys., 243, 19
- De Pontieu, B. et al. 2007, Science, 318, 1574
- Dere, K. P., Landi, E., Mason, H. E., Fossi, B. C. M., & Young, P. R. 1997, A&AS, 125, 149
- Dolla, L. & Solomon, J. 2008, A&A, 483, 271
- Doyle, J. G., Banerjee, D., & Perez, M. E. 1998, Sol. Phys., 181, 91
- Doyle, J. G., Teriaca, L., & Banerjee, D. 1999, A&A, 349, 956
- Esser, R. et al. 1999, ApJ, 510, 63
- Goossens, M., Erdélyi, R., & Ruderman, M. S. 2011, Space Sci. Rev., 158, 289

- Goossens, M., Terradas, J., Andries, J., Arregui, I., & Ballester, J. L. 2009, *A&A*, 503, 213
- Guhathakurta, M., Rottman, G. J., Fisher, R. R., Orrall, F. Q., & Alrock, R. C. 1992, *ApJ*, 388, 633
- Hahn, M., Bryans, P., Landi, E., Miralles, M. P., & Savin, D. W. 2010, *ApJ*, 725, 774
- Hahn, M., Landi, E., & Savin, D. W. 2012, *ApJ*, 753, 36
- Hahn, M. & Savin, D. W. 2013, *ApJ*, 763, 106
- Heyvaerts, J. & Priest, E. R. 1983, *A&A*, 117, 220
- Jess, D. B. et al. 2009, *Science*, 323, 1582
- Kamio, S., Hara, H., Watanabe, T., & Hansteen, V. H. 2010, *SolPhys*, 266, 209
- Kosugi, T. et al. 2007, *Sol. Phys.*, 243, 3
- Landi, E. & Cranmer, S. R. 2009, *ApJ*, 691, 794
- Landi, E., Del Zanna, G., Young, P. R., Dere, K. P., & Mason, H. E. 2012, *ApJ*, 744, 99
- Leamon, R. J., Smith, C. W., Ness, N. F., Matthaeus, W. H., & Wong, H. K. 1998, *JGR*, 103, 4775
- Matthaeus, W. H., Zank, G. P., Oughton, S., Mullan, D. J., & Dmitruk, P. 1999, *ApJ*, 523, 93
- McComas, D. J., Ebert, R. W., Elliot, H. A., Goldstein, B. E., Gosling, J. T., Schwadron, N. A., & Skoug, R. M. 2008, *Geophys. Res. Lett.*, 35, 18103
- McIntosh, S. W. et al. 2011, *Nature*, 475, 477
- Moran, T. G. 2001, *A&A*, 374, L9

- . 2003, *ApJ*, 598, 657
- O’Shea, E., Banerjee, D., & Doyle, J. G. 2005, *A&A*, 436, L35
- Parker, E. N. 1991, *ApJ*, 372, 719
- Phillips, K. J. H., Feldman, U., & Landi, E. 2008, *Ultraviolet and X-ray Spectroscopy of the Solar Atmosphere* (Cambridge University Press)
- Podesta, J. J., Roberts, D. A., & Goldstein, M. L. 2007, *ApJ*, 664, 543
- Tomczyk, S. et al. 2007, *Science*, 317, 1192
- Tu, C.-Y., Marsch, E., Wilhelm, K., & Curdt, W. 1998, *ApJ*, 503, 475
- Ugarte, I. 2010, EIS Software Note No. 12:
[http://hesperia.gsfc.nasa.gov/ssw/hinode/eis/doc/
eis_notes/12_STRAY_LIGHT/eis_swnote_12.pdf](http://hesperia.gsfc.nasa.gov/ssw/hinode/eis/doc/eis_notes/12_STRAY_LIGHT/eis_swnote_12.pdf)
- Van Doorselaere, T., Nakariakov, V. M., & Verwichte, E. 2008, *ApJ*, 676, L73
- Wang, Y.-M. 2010, *ApJ*, 715, L121
- Wang, Y.-M., Robbrecht, E., & Sheeley, Jr., N. R. 2009, *ApJ*, 707, 1372
- Wilhelm, K. et al. 2011, *Astron. Astrophys. Rev.*, 19, 35
- Withbroe, G. L. & Noyes, R. 1977, *ARA&A*, 15, 363
- Young, P. 2011, EIS Software Note No. 7:
[http://hesperia.gsfc.nasa.gov/ssw/hinode/eis/doc/eis_notes/
eis_notes/07_LINE_WIDTH/eis_swnote_07.pdf](http://hesperia.gsfc.nasa.gov/ssw/hinode/eis/doc/eis_notes/eis_notes/07_LINE_WIDTH/eis_swnote_07.pdf)